Appl. Phys. A 55, 279–288 (1992)

Contactless Measurement of the Conductivity of II–VI Epitaxial Layers by Means of the Partially Filled Waveguide Method

P. Greiner, L. Polignone, C. R. Becker, and R. Geick

Physikalisches Institut der Universität Würzburg, W-8700 Würzburg, Fed. Rep. Germany, (Fax: +49-931/888-5142)

Received 6 March 1992/Accepted 2 June 1992

Abstract. We report the contactless determination of the conductivity, the mobility and the carrier concentration of II–VI semiconductors by means of the technique of the partially filled waveguide at a microwave frequency of 9 GHz. The samples are CdHgTe epitaxial layers, grown on CdZnTe substrates by molecular beam epitaxy. The conductivity is determined from the transmission coefficient of the sample in the partially filled waveguide. For the analysis of the experimental data, the complex transmission coefficient is calculated by a rigorous multi-mode matching procedure. By varying the conductivity of the sample, we obtain an optimum fit of the calculated data to the experimental results. Comparison with conductivity data determined by the van der Pauw method shows that our method allows to measure the conductivity with good accuracy. The behaviour of the transmission coefficient of the sample is discussed in dependence on the layer conductivity, the layer thickness and the dielectric constant of the substrate. The calculations require to consider in detail the distribution of the electromagnetic fields in the sample region. The usual assumption of a hardly disturbed TE_{10} mode cannot be used in our case. By applying a magnetic field in extraordinary Voigt configuration, galvanomagnetic measurements have been carried out which yield the mobility and thus the carrier concentration. These results are also in good agreement with van der Pauw transport measurements.

PACS: 72.20.–i, 72.80.Ey, 78.70.Gq

There is a growing interest in II–VI semiconductors because of their potential applications as devices in the areas of opto-electronics and photonics. Their bandgap spans a wide range from the infrared (CdHgTe) to the violet (ZnS). Consequently, some members of this semiconcutors family are used as sensitive infrared detectors while others will be suitable for the realization of LED's etc. with light emission in the blue part of the visible spectrum. But a number of technical problems have to be overcome before we know how to fabricate reliable devices of this kind. A major step towards solving these problems is the growth of high quality epitaxial films by means of a new, recently developed growth process, namely photoassisted molecular beam epitaxy (PAMBE) [1, 2]. The growth of such films has always been difficult because of the tendency of II–VI compounds to incorporate local defects such as vacancies, interstitials and impurities [3]. After the growth of the epitaxial layers, it is absolutely necessary to characterize the samples, i.e. to measure the conductivity, the Hall effect etc., in order to control and optimize their quality with sufficient accuracy in a short time. The knowledge of the electrical transport parameters is especially required in the field of device fabrication. Unfortunately, that is often hampered by the fact that it is difficult or sometimes even impossible to obtain good ohmic contacts. One reason for this is the well known tendency of self-compensation in II–VI compounds.

To avoid these problems, a useful alternative is the contactless measurement by means of microwave methods. For small or thin needle-shaped samples, transmission or reflection cavities are usually used to obtain information about the conductivity of semiconductors [4–6]. The Hall effect has been investigated by employing bimodal cavities [7]. For large samples which fill a rectangular wave-guide totally or which are at least large enough to cover the waveguide cross-section, it is appropriate to measure the reflection or the transmission coefficient of the sample. Concerning dielectric materials, a large number of methods for measuring reflection or transmission can be found in the standard literature of microwave techniques [8]. Many of these methods have also been applied for the characterization of semiconductors, e.g., for the determination of the dielectric constant of silicon [9] or of the conductivity and mobility of GaAs layers [10]. Even the quantum Hall effect has been investigated on GaAs/GaAlAs heterostructures by the crossed waveguide method [11, 12]. Another field of the application of microwave methods are measurements of the transport properties where the main interest is to study the relative changes of the transport quantities, e.g. cyclotron resonances, and not to obtain their absolute values. One example of this kind is the investigation of the voltage and magnetic field dependence of the conductivity in MOSFETS [13, 14].

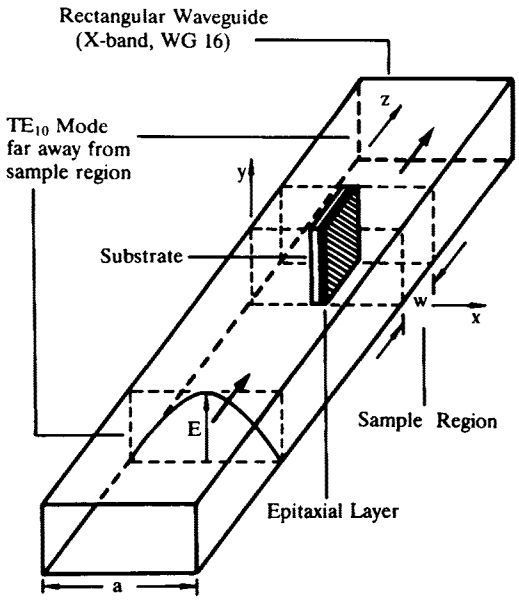

Fig. 1. The partially filled waveguide with the sample in upright position near the center

From the beginning of our experiments on epitaxial layers of II–VI semiconductors, we aimed at the accurate determination of the absolute values of the transport properties such as conductivity, mobility and carrier concentration. In our case, the epitaxial layers with a thickness between 1 μm and 5 μm are grown on $Cd_{0.96}Zn_{0.04}Te$ substrates with dimensions 10 mm × 5 mm × 1 mm. These samples fit very well into a rectangular X-band waveguide in the way shown in Fig. 1. The layer conductivities range between $1\,(\Omega\,\mathrm{cm})^{-1}$ and $3000\,(\Omega\,\mathrm{cm})^{-1}$. To reach our goal for this wide range of conductivities, we found the method of the partially filled waveguide the most appropriate, among a large variety of microwave methods. In this method, the sample is inserted in the center of a rectangular standard waveguide (see Fig. 1) and the conductivity of the layer is deduced from the attenuation and the phase shift of the microwave which has passed the sample. This procedure requires one to measure the complex transmission coefficient of the sample region (cf. Fig. 1) and to compare it to calculated data, where the conductivity of the sample is varied until an agreement is reached. A second requirement is to know in advance the conductivity and the dielectric constant of the substrate which also has a perceptable influence on the experimental data. For the calculation often the assumption is employed, that the TE_{10} mode is hardly disturbed by the sample. The TE_{10} mode is the only propagating mode in the empty waveguide for the frequency range between 8 GHz and 12 GHz. The condition of a nearly undisturbed TE_{10} mode is only fulfilled if the thickness of the sample is sufficiently small in relation to its dielectric constant. In this way, investigations of the dielectric constant of BaF_2–PbSnTe–BaF_2 sandwich structures [15, 16] have been performed. In our case, however, it will turn out that the assumption of a nearly undisturbed TE_{10} mode is not justified for layers with conductivities above $100\,(\Omega\,\mathrm{cm})^{-1}$. If we, nevertheless, analyse our data using this assumption, the results are not in agreement with usual transport measurements. Obviously, the conductivities of the samples and thus the imaginary part of the dielectric constant are so high that the TE_{10} mode is strongly distorted. Therefore, we had to apply a more sophisticated theory which describes the distortion of the propagating mode by calculating the distribution of the electromagnetic fields in the sample region using a large number of modes in a multimode analysis.

In the next section, we will describe the theoretical considerations with the multi-mode matching procedure. The following sections are devoted to the microwave equipment as it was used in the experiments and to the experimental results including galvanomagnetic measurements, which yield the mobility of the carriers and the carrier concentration by using a simple one carrier model.

1 Theoretical Considrations

1.1 Transmission Coefficient

In this section, the mathematical procedure will be derived which is used to calculate the transmission coefficient (modulus and phase). The results of this calculation are then compared to the experimental data and an optimum fit is obtained by varying the conductivity of the layer as an input parameter.

A number of possible ways to do this calculation have been reported in the literature. The problem of the partially filled waveguide has been of interest for many years because of its great importance in microwave techniques, e.g. in the construction of devices such as phase shifters, polarization converters, attenuators and filters. One of the most frequently applied methods in dealing with the discontinuity, corresponding to our sample in the waveguide, is the variational principle combined with an equivalent network analysis [17], especially for dielectric or metallic posts [18, 19]. If the samples have dimensions comparable to the wavelength of the microwave, these problems are often studied with the finite element or the effective dielectric constant method [20]. Recently, combinations of network analysis with other theoretical approaches have been reported [21]. Xu Shanjia introduced a method which combines rigorous multi-mode matching with the multi-mode network theory [22]. So far, all these methods have been applied mostly to bulk dielectric material with very small imaginary components of the dielectric constant or to metallics.

In contrast to the above mentioned methods of network analysis using the equivalent network theory, we start from the propagation of electromagnetic waves directly. This method is very clear because the whole field distribution and the transmission and reflection coefficients are built up step by step while maintaining the same accuracy as the network analysis. Figure 2 shows a cross-section of the waveguide with the sample located at the position a_1, the substrate located in the segment between a_1 and a_2, and the layer between a_2 and a_3. The segments 1 and 4 are empty, i.e. filled with air. Input parameters for our calculation are the effective dielectric constants $\hat{\varepsilon}_E$ and $\hat{\varepsilon}_S$, the thicknesses $d_E = a_3 - a_2$ and $d_S = a_2 - a_1$ of the epitaxial layer (subscript "E") and of the substrate (subscript "S"), respectively, the microwave frequency f, the length w of the sample and its position in the waveguide. The effective complex dielec-

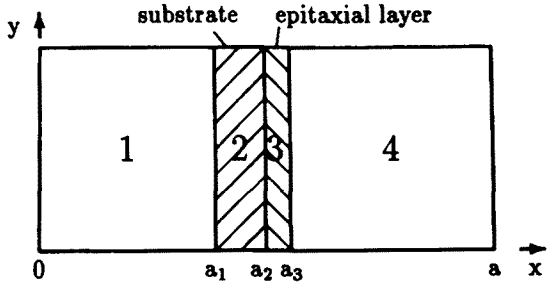

Fig. 2. Waveguide cross-section in the sample region. The different segments are denoted by 1–4, their interfaces being at $x = a_1$, a_2, and a_3

tric constants combine the effects of the lattice and of the free carriers:

$$\hat{\varepsilon}_{S/E} = \varepsilon_{\text{lattice, S/E}} - \frac{\sigma_{S/E}\tau_{S/E}}{\varepsilon_0[1 + (\omega\tau_{S/E})^2]} - \frac{i\sigma_{S/E}}{\omega\varepsilon_0[1 + (\omega\tau_{S/E})^2]}, \quad (1)$$

where the static dielectric constants $\varepsilon_{\text{lattice, S/E}}$ are assumed to be real and frequency independent. The dc-conductivities $\sigma_{S/E}$ are isotropic. In addition, $\tau_{S/E}$ is the relaxation time and $\omega = 2\pi f$ (microwave frequency). The samples are assumed to be nonmagnetic with the relative magnetic permeability $\hat{\mu} = 1$. Among the input parameters listed above, the quantities w, d_S, a_1, and f are fixed according to the experimental conditions. As already mentioned, the effective dielectric constant $\hat{\varepsilon}_S$ (substrate) has to be measured before growing the epitaxial layers. The thickness d_E of the epitaxial layer is determined independently by Fourier transform spectroscopy and by X-ray diffraction. Finally, $\hat{\varepsilon}_E$ of the layer is obtained from the fit procedure, where $\varepsilon_{\text{lattice, E}}$ [cf. (1)] is taken into account by inserting an appropriate value.

The first step in the calculation is to describe the electromagnetic fields in and near the sample region. The sample fills the rectangular waveguide in the y-direction (see Fig. 2) and is assumed to fill it completely. Thus, the solution of the problem will not depend on y. Far away from the sample, there will be a pure TE_{10} mode propagating in z-direction (cf. Fig. 1). But near the sample, the electromagnetic field will be composed of a number of modes because of the distortion of the TE_{10} mode by the sample. For reasons of symmetry (no y-dependence), the modes near the sample but outside the sample region in the empty waveguide will be TE_{m0} modes, where the field components of the mth mode can be written as:

$$\left.\begin{aligned} E_y^m &= -iCH_{m0}G_{m0}\exp(-iq_m z), \\ H_x^m &= iH_{m0}q_m G_{m0}\exp(-iq_m z), \\ H_z^m &= H_{m0}G'_{m0}\exp(-iQ_m z), \end{aligned}\right\} \quad (2)$$

with

$$G_{m0} = G_{m0}(x) = (a/m\pi)\sin(m\pi x/a)\exp(i\omega t),$$
$$G'_{m0} = G'_{m0}(x) = \cos(m\pi x/a)\exp(i\omega t).$$

In (2), q_m is the propagation constant with $q_m^2 = (\omega/c)^2 - (m\pi/a)^2$ and C is the abbreviation for $C = (\omega/c)(\mu_0/\varepsilon_0)^{1/2}$.

For the partially filled waveguide, i.e. the sample region (cf. Fig. 1, $0 \le z \le w$), the electromagnetic field will be composed of a number of modes of a different type. These modes are solutions of the Maxwell's equations when we take into account the boundary conditions between the segments 1–4 (cf. Fig. 2) and at the wall of the waveguide. The symmetry of the problem allows the modes to be TE_{m0}-like. Then, the field components of the jth mode are defined for each of the segments $\alpha = 1, 2, 3, 4$ as follows:

$$\left.\begin{aligned} E_{y,\alpha}^j &= -i(C/\tilde{q}_{\alpha,j})H_{\alpha,j}\sin(\tilde{q}_{\alpha,j}x + \varphi_{\alpha,j}) \\ &\quad \times \exp[i(\omega t - \hat{q}_j z)], \\ H_{x,\alpha}^j &= i(\hat{q}_j/\tilde{q}_{\alpha,j})H_{\alpha,j}\sin(\tilde{q}_{\alpha,j}x + \varphi_{\alpha,j}) \\ &\quad \times \exp[i(\omega t - \hat{q}_j z)], \\ H_{z,\alpha}^j &= H_{\alpha,j}\cos(\tilde{q}_{\alpha,j}x + \varphi_{\alpha,j}) \\ &\quad \times \exp[i(\omega t - \hat{q}_j z)], \end{aligned}\right\} \quad (3)$$

with

$$\tilde{q}_{\alpha,j}^2 = \hat{\varepsilon}_\alpha(\omega/c)^2 - \hat{q}_j^2,$$

where $\hat{q}_j$ is the complex propgation constant for the jth mode. The different solutions for $\hat{q}_j$ and thus the different possible modes j in the sample region are calculated by using the boundary conditions, i.e. continuity of E_y, B_x, and H_z in the transversal x-direction at a_1, a_2, and a_3. These conditions lead to a homogeneous system of linear equations for $H_{\alpha,j}\sin\varphi_{\alpha,j}$ and $H_{\alpha,j}\cos\varphi_{\alpha,j}$. Solving the transcendental secular equation of this system yields $\hat{q}_j$ and the eigenvectors, and consequently, the amplitudes $H_{\alpha,j}$ and the phase angles $\varphi_{\alpha,j}$.

The second step is to relate the modes in the sample region to the modes outside this region by means of the boundary conditions at $z = 0$ and $z = w$. In this procedure, the j modes in the sample region are expressed as TE_{m0} modes of the empty waveguide by means of a Fourier analysis. We can then describe the field distributions inside and outside the sample region in terms of the same TE_{m0} modes which are known to form a complete set of orthonormal functions.

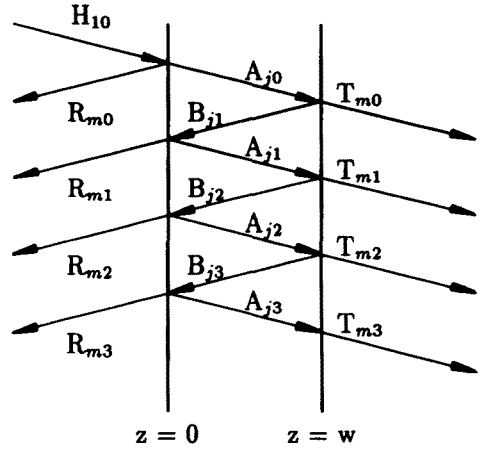

Fig. 3. Amplitudes of the mode incident on the sample and of the modes reflected and transmitted at the interfaces at $z = 0$ and $z = w$, respectively, including multiple reflections. For reasons of clarity, we have drawn a finite angle of incidence which is zero in reality

This method with the Fourier analysis facilitates the mode matching in which we have to match the field distributions inside and outside of the sample region. We can now treat the boundary conditions for each TE_{m0} mode separately. In principle, an infinite set of modes has to be used for these calculations, but we shall restrict ourselves to a finite number of modes which is large enough to describe the actual field distribution across the waveguide sufficiently well.

It is assumed that a TE_{10} mode propagating in the z-direction with amplitude H_{10} is incident to the sample region at $z = 0$. According to the scheme in Fig. 3, the reflected wave consists of TE_{m0} modes with coefficients R_{mk} and the transmitted part of the j modes (sample region) with coefficients A_{jk}, where k is the order of zig-zag-reflections in the sample. At $z = w$, the incident wave consists of modes with coefficients A_{jk}. The transmitted parts are TE_{m0} modes with coefficients T_{mk} and the reflected parts the j modes with coefficients $B_{j(k+1)}$ propagating in the negative z-direction. In this way, the total field distribution inside and outside the sample region is built up step by step as shown by the arrows in Fig. 3, starting with $k = 0$. The final result is given by the following expressions for the field components:

a) for $z \leq 0$ (before the sample region):

$$
\begin{aligned}
E_y &= -\mathrm{i}C \sum_m \left(H_{10}\delta_{m,1} + \sum_k R_{mk} \right) \\
&\quad \times G_{m0} \exp(-\mathrm{i}q_m z)\,, \\
H_x &= \mathrm{i} \sum_m \left(H_{10}\delta_{m,1} + \sum_k R_{mk} \right) \\
&\quad \times q_m G_{m0} \exp(-\mathrm{i}q_m z)\,, \\
H_z &= \sum_m \left(H_{10}\delta_{m,1} + \sum_k R_{mk} \right) \\
&\quad \times G'_{m0} \exp(-\mathrm{i}q_m z)\,;
\end{aligned}
\tag{4}
$$

b) for $0 \leq z \leq w$ (sample region):

$$
\begin{aligned}
E_y &= -\mathrm{i}C \sum_m G_{m0} \Big\{ \sum_j F_{mj} \sum_k [A_{jk} \exp(-\mathrm{i}\hat{q}_j z) \\
&\quad + B_{jk} \exp(\mathrm{i}\hat{q}_j z)] \Big\}, \\
H_x &= \mathrm{i} \sum_m G_{m0} \Big\{ \sum_j F_{mj} \cdot \hat{q}_j \sum_k [A_{jk} \exp(-\mathrm{i}\hat{q}_j z) \\
&\quad - B_{jk} \exp(\mathrm{i}\hat{q}_j z)] \Big\}, \\
H_z &= \sum_m G'_{m0} \Big\{ \sum_j F_{mj} \sum_k [A_{jk} \exp(-\mathrm{i}\hat{q}_j z) \\
&\quad + B_{jk} \exp(\mathrm{i}\hat{q}_j z)] \Big\};
\end{aligned}
\tag{5}
$$

c) for $z \geq w$ (after the sample region):

$$
\begin{aligned}
E_y &= -\mathrm{i}C \sum_m \left(\sum_k T_{mk} \right) G_{m0} \exp(-\mathrm{i}q_m z)\,, \\
H_x &= \mathrm{i} \sum_m \left(\sum_k T_{mk} \right) q_m G_{m0} \exp(-\mathrm{i}q_m z)\,, \\
H_z &= \sum_m \left(\sum_k T_{mk} \right) G'_{m0} \exp(-\mathrm{i}q_m z)\,.
\end{aligned}
\tag{6}
$$

In (5), the factors F_{mj} are the Fourier coefficients of the jth mode in the sample region with respect to the mth mode of the empty waveguide according to the above mentioned Fourier analysis. The longitudinal boundary conditions, namely continuity of E_y, H_x, and B_z at $z = 0$ and at $z = w$, lead to an inhomogeneous system of linear equations which allows us to evaluate all coefficients A_{jk}, B_{jk}, R_{mk}, and T_{mk} as quantities proportional to H_{10}, the amplitude of the incident wave. As already pointed out, this calculation can be performed only for a finite number of modes N which means that m and j are restricted according to $1 \leq m \leq N$ and $1 \leq j \leq N$, respectively. This inhomogeneous set of linear equations may be expressed in matrix form, where we define the following N-dimensional vectors as well as specify their components in brackets:

$$
\left.
\begin{aligned}
&\mathbf{H}_0 \;\; [H_{10}\delta_{m,1};\; k = 0 \text{ only!}]\,, && \mathbf{R}_k \;\; [R_{mk}]\,, \quad \mathbf{T}_{mk} \;\; [T_{mk}]\,, \\
&\mathbf{A}_k \;\; [A_{jk} \exp(-\mathrm{i}2k\hat{q}_j w)]\,, && \mathbf{B}_k \;\; [B_{jk} \exp(-\mathrm{i}2k\hat{q}_j w);\; B_{j0} \equiv 0]\,, \\
&\mathbf{A}'_k \;\; [A_{jk} \exp(-\mathrm{i}[2k+1]\hat{q}_j w)]\,, && \mathbf{B}'_k \;\; [B_{jk} \exp(-\mathrm{i}[2k-1]\hat{q}_j w);\; B_{j0} \equiv 0]\,.
\end{aligned}
\right\}
\tag{7}
$$

Similarly, we define the following $N \times N$ matrices and their elements in brackets:

$$
(F^+) \;\; [(1 + \hat{q}_j/q_m)F_{mj}]\,, \qquad (F^-) \;\; [(1 - \hat{q}_j/q_m)F_{mj}]\,. \tag{8}
$$

With these definitions, the inhomogeneous system of linear equations representing the boundary conditions reads in matrix form as follows:

a) $z = 0$

$$
\left.
\begin{aligned}
&(F^+) \;\; \mathbf{A}_k + (F^-)\mathbf{B}_k = 2\mathbf{H}_0\delta_{k,0}\,, \\
&(F^-) \;\; \mathbf{A}_k + (F^+)\mathbf{B}_k = 2\mathbf{R}_k\,;
\end{aligned}
\right\}
\tag{9}
$$

b) $z = w$

$$
\left.
\begin{aligned}
&(F^-) \;\; \mathbf{A}'_k + (F^+)\mathbf{B}'_k = 0\,, \\
&(F^+) \;\; \mathbf{A}'_k + (F^-)\mathbf{B}'_k = 2\mathbf{T}_k\,.
\end{aligned}
\right\}
\tag{10}
$$

For each value of k (cf. Fig. 3), there are two sets of matrix equations for $z = 0$ [see (9)] and two sets for $z = w$ [see (10)]. The calculation starts with $k = 0$ to determine $\mathbf{A}_0$ and $\mathbf{R}_0$ from $\mathbf{H}_0$ by means of (9), where $\mathbf{B}_0 \equiv 0$. The next steps are to calculate successively $\mathbf{B}'_{(k+1)}$ and $\mathbf{T}_k$ from $\mathbf{A}'_k$ (10) for each value of k starting with $k = 0$, and then $\mathbf{A}_k$ and $\mathbf{R}_k$ from $\mathbf{B}_k$ (9). It is evident from (7) that $\mathbf{A}_k$ and $\mathbf{A}'_k$ and as well as $\mathbf{B}_k$ and $\mathbf{B}'_k$ differ only by a phase factor and are otherwise identical. This procedure is continued until k is large enough, i.e. more reflections back and forth do not contribute significantly to the signal. Near the sample region, the transmitted signal consists of a number of TE_{m0} modes with amplitudes T_{mk} added up for all values of k (see Fig. 3). Far away from the sample, however, only the propagating TE_{10} mode persists and the measured transmission signal is

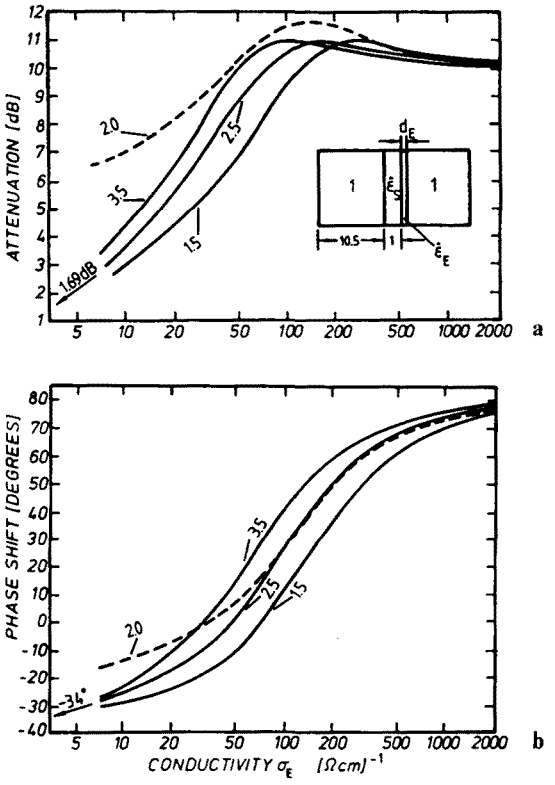

Fig. 4a, b. Calculated transmission coefficient, i.e. attenuation (**a**) and phase shift (**b**), evaluated for $\hat{\varepsilon}_S = 11.0 - 0.5\,i$ and for various layer thicknesses d_E (full lines, d_E in μm as a parameter) and for $\hat{\varepsilon}_S = 10.6 - 11.0\,i$ and $d_E = 2.0\,\mu m$ (broken line). For further explanations and values of the other parameters see text

therefore

$$T = \sum_k T_{1k} . \tag{11}$$

As a reference, we consider the corresponding transmission signal of the empty waveguide which is

$$T_0 = H_{10} \exp(-iq_1 w) .$$

The complex transmission coefficient of the sample is then the ratio of T and T_0. Its modulus $A = |T/T_0|$ is the attenuation of the microwave caused by the sample. The attenuation will usually be expressed in decibels (dB). The phase shift originating from the sample is $\varphi = arc(T/T_0)$, which will be expressed in degrees.

For the analysis of the experimental data, it is very useful and is found to be the most appropriate representation when A and φ are plotted as a function of the conductivity σ_E of the layer. An example is shown in Fig. 4. Values of the experimental parameters used in all calculations are compiled in Table 1. The value for $\hat{\varepsilon}_S$ is given in Fig. 4. In calculating $\hat{\varepsilon}_E$ from σ_E, we have used $\varepsilon_{\text{lattice, E}} = 20.0$ for the lattice contribution to $\hat{\varepsilon}_E$. This value for $\varepsilon_{\text{lattice, E}}$ is discussed in detail below in context with Table 2. The curves in Fig. 4 show a large increase in A with increasing layer conductivity for $\sigma_E < 100\,(\Omega\,cm)^{-1}$. At higher values of σ_E, A reaches a maximum and is then nearly independent of the conductivity. The phase shift φ, on the other hand, varies strongly with the layer conductivity for values between $20\,(\Omega\,cm)^{-1}$ and $1000\,(\Omega\,cm)^{-1}$. This means we can use both A and φ for the determination of σ_E when $\sigma_E < 100\,(\Omega\,cm)^{-1}$. For $\sigma_E > 100\,(\Omega\,cm)^{-1}$, on the other hand, it is more appropriate to use only φ for this purpose. Furthermore, both quantities, i.e. A and φ, also depend strongly on the layer thickness d_E as is evident from the various curves (full lines) in Fig. 4 with d_E as parameter. Also the influence of $\hat{\varepsilon}_S$ of the substrate is illustrated in Fig. 4 (broken line, $d_E = 2\,\mu m$). Therefore, these two parameters have to be known with good accuracy when the layer conductivity is to be deduced from the experimental data. The transmission coefficient of the sample and also the reflection coefficient depend, additionally, on quantities such as frequency or sample length w. These dependences will be discussed in a forthcoming paper [23].

Table 1. Values of the parameters which are fixed by the experimental conditions and which were used in all calculations without variation

Sample position (cf. Fig. 2)	$a_1 = 10.5$ mm
Sample length (cf. Fig. 1)	$w = 5.0$ mm
Substrate thickness	$d_S = 1.0$ mm
Microwave frequency	$f = 8.9$ GHz

The behaviour of the transmission coefficient, as demonstrated in Fig. 4, results from the field distributions near the sample in the waveguide. The field distributions are clear evidence that the nearly undisturbed TE_{10} mode is not a good approximation in the case of our samples. For low layer conductivities, the dominant effects are due to the substrate with its relatively high dielectric constant (real part of $\hat{\varepsilon}_S$). Therefore, the whole electric field is more or less concentrated in the substrate [see Fig. 5a for a low layer conductivity of $\sigma_E = 9.1\,(\Omega\,cm)^{-1}$]. For more clarity, only the modulus $|\mathbf{E}_y|$ of the electric field is shown in Fig. 5 with its variation over the waveguide cross-section (x-dependence) for various values of z in the sample region ($0 \leq z \leq w$) and beyond ($z \geq w$). At some distance beyond the sample, only the TE_{10} mode will be found since all the other modes are cut-off modes and die out within about 10 mm. When the layer conductivity increases above the value demonstrated in Fig. 5a, the microwave properties of the sample will be dominated more and more by the layer conductivity. for conductivities larger than $500\,(\Omega\,cm)^{-1}$, the field at the sample position will approach zero and, thus, the field configuration is practically that of a metallic strip in the center of the waveguide. An example of a field distribution in and near a sample with high conductivity ($\sigma_E = 500\,(\Omega\,cm)^{-1}$) is shown in Fig. 5b. A comparison shows that the transmission coefficient is considerably smaller for the sample with higher conductivity ($|T/T_0| = 0.304$ in Fig. 5b) then for the sample with the lower conductivity ($|T/T_0| = 0.706$ in Fig. 5a) for the reasons discussed above. There is also a drastic change in phase shift between the two sample, namely from $\varphi = -61.93°$ in Fig. 5a to $\varphi = 34.95°$ in Fig. 5b.

1.2 Galvanomagnetic Measurements

Our experimental equipment (see next section) enables us to study the conductivity of our samples as a function of tem-

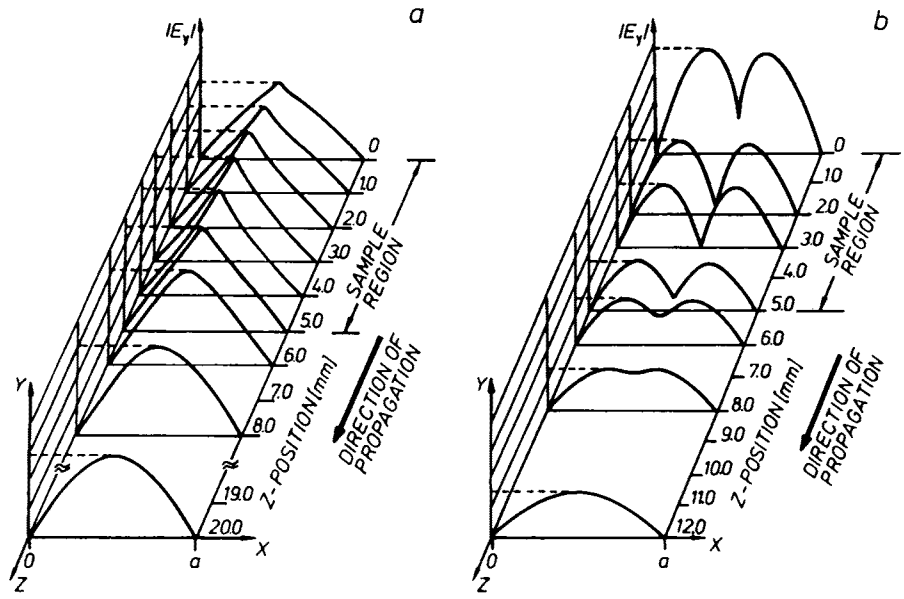

Fig. 5a, b. Field distribution in and beyond the sample region for a layer conductivity of **a** $\sigma_E = 9.1\,(\Omega\,\mathrm{cm})^{-1}$ and **b** $\sigma_E = 500\,(\Omega\,\mathrm{cm})^{-1}$. The values of the other parameters are $\hat{\varepsilon}_S = 11.0 - 0.8\,\mathrm{i}$ and $11.0 - 0.5\,\mathrm{i}$, $d_E = 2.0\,\mu\mathrm{m}$ and $3.0\,\mu\mathrm{m}$, $N = 20$ modes and 70 modes for **a** and **b**, respectively. For more clarity, we present only the modulus $|E_y|$ as a function of x at various positions z

perature and an external magnetic field. The magnetic field with a strength up to 0.6 T was applied in the x-direction (see Fig. 6). Following the classification in the literature, this arrangement is called an extraordinary Voigt configuration [24], where the layer conductivity becomes a tensor of the following form

$$\hat{\sigma} = \begin{pmatrix} \hat{\sigma}_{xx} & 0 & 0 \\ 0 & \hat{\sigma}_{yy} & \hat{\sigma}_{yz} \\ 0 & -\hat{\sigma}_{yz} & \hat{\sigma}_{zz} \end{pmatrix} \tag{12}$$

with

$$\hat{\sigma}_{yy} = \hat{\sigma}_{zz} = \sigma_E[1 - \mathrm{i}\omega\tau_E]/[1 + (\mu_E B)^2]\,, \tag{13}$$

$$\hat{\sigma}_{yz} = \sigma_E(\mu_E B)[1 - \mathrm{i}\omega\tau_E]/[1 + (\mu_E B)^2]\,, \tag{14}$$

$$\hat{\sigma}_{xx} = \sigma_E = e n_E \mu_E\,. \tag{15}$$

Here, μ_E is the mobility of the carriers in the layer, n_E their concentration and B the applied magnetic field. In (13)–(15), it is assumed that $(\omega\tau_E)^2 \ll 1$ and can be neglected (see below). For further details, the reader is referred to the literature [24, 25]. According to (1), the effective dielectric constant $\hat{\varepsilon}_E$ becomes a tensor of the same form as the tensor of the conductivity $\hat{\sigma}$ (12). When a sample contains several types of carriers denoted by k, the components of the conductivity tensor become

$$\hat{\sigma}_{ij} = \sum_k \hat{\sigma}_{ij}^k\,. \tag{16}$$

Now, the assumption is made that only a small and negligible E_z component of the electric field arises as a consequence of the magnetic field and of the resulting Hall effect. Neglecting thus the change in the field distribution originating from E_z, we have determined the conductivity of the sample, in particular of the epitaxial layer, in the way described above for the case without magnetic field. This means, we have measured the diagonal component $\hat{\varepsilon}_{yy}$ of the dielectric tensor under these conditions and, correspondingly, the component $\hat{\sigma}_{yy}$ of the conductivity tensor. On the other hand, we would not be able to observe the change in field distribution with our equipment, namely the TM_{mn} modes with an E_z component of the electric field, because these are not propagating modes in our waveguide.

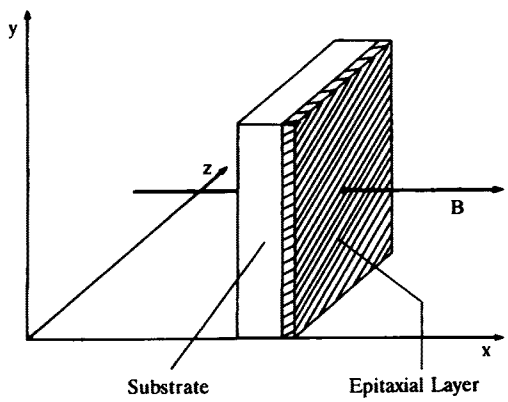

Fig. 6. Configuration of the sample in the external magnetic field

2 Experimental Procedure

The experimental equipment (see Fig. 7) consists of a microwave bridge [16] in standard rectangular waveguide technique for the X-band (8.2 GHz–12.4 GHz). The microwave radiation emitted by the Gunn oscillator is divided by a 3 dB directional coupler and half of the power is sent through the sample channel and the other half through the reference channel. By a second directional coupler, the radiation of both channels is recombined and guided to the detector. The transmission coefficient is measured by equalizing the bridge, i.e. zero signal at the detector. This is performed twice by means of the attenuator and the phase shifter for:

a) the empty transmission line and

b) the sample in the transmission line.

The differences in the setting of the attenuator and of the phase shifter yield then the transmission coefficient of the

sample. The four isolators in the microwave bridge ensure that the microwaves can propagate only in forward direction and that the measurements are not obscured by reflected waves propagating in the opposite direction. The typical frequency for our measurements has been 8.9 GHz, where the VSWR (voltage standing wave ratio) is lower than 1.1 in our set-up. In contrast to usual microwave bridges, our equipment includes a 1 T electromagnet and a cryostat which has been constructed especially for the microwave bridge and which allows continuous temperature dependent measurements between 4.2 K and 300 K.

3 Analysis of the Experimental Data

All our samples are epitaxial layers of II–VI semiconductors grown on commercially available $Cd_{0.96}Zn_{0.04}Te$ substrates by MBE (molecular beam epitaxy). In Table 2, we have compiled the electrical properties of the samples studied by our microwave method. The values for $\hat{\varepsilon}_S$ of the substrates have been determined by the microwave method before growing the epitaxial layers. The real part of $\hat{\varepsilon}_S$ is essentially due to the lattice contribution $\varepsilon_{\text{lattice, S}}$. It decreases linearly with decreasing temperature. Our values are in good agreement with data obtained by other methods [26]. The imaginary part of $\hat{\varepsilon}_S$ results from the conductivity of the substrate material. The conductivity varies between 0.0025 and 0.055 $(\Omega\,\text{cm})^{-1}$ at room temperature depending on the particular substrate (cf. Table 2) thus showing that a number of substrates do not fulfill the requirement of a high resistivity. Also, the structural quality is often not quite satisfactory [27]. The values of the conductivity σ_E of the epitaxial layers compiled in Table 2 were determined at room temperature by the van der Pauw method [28] which is fairly reliable for our samples which all are n-type. From the conductivity σ_E (cf. Table 2), we have calculated the effective dielectric constant $\hat{\varepsilon}_E$ for the epitaxial layers [cf. (1)], where we have used for the relaxation time a typical value of 5×10^{-13} s and for the lattice contribution to $\hat{\varepsilon}_E$ the value $\varepsilon_{\text{lattice, e}} = 20,0$ for all HgCdTe samples listed in Table 2. This is actually the value for pure HgTe [29]. Since our samples have relatively small Cd-concentrations (cf. Table 2) and since the microwave properties of the layers are clearly dominated by their conductivity (imaginary part of $\hat{\varepsilon}_E$), only a negligible error is introduced by using this value for all samples instead of a more accurate individual value for each sample [29]. Finally, it turns out in these calculations that the condition $(\omega\tau)^2 \ll 1$ is always fulfilled for the microwave frequencies under consideration and that we measure more or less the dc-conductivity with the microwave bridge.

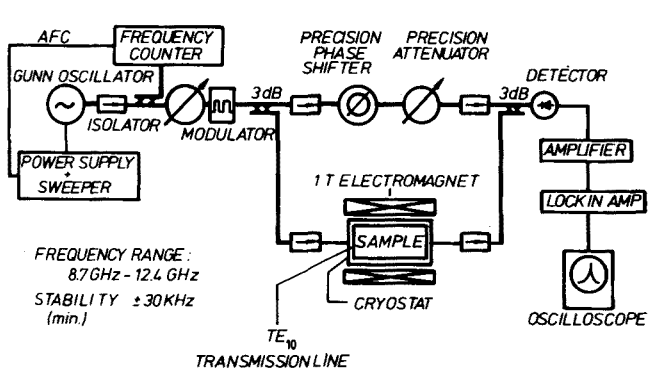

Fig. 7. The microwave bridge with the TE_{10} transmission line, combined with a cryostat and a 1 T electromagnet

Table 2. Properties of the epitaxial layers: All the layers are grown on $Cd_{0.96}Zn_{0.04}Te$ substrates. CMT xx and Q xxx are internal denotations for the samples. The number in brackets denote the Cd-concentration. Samples CMT 78 and Q 132 are superlattices

Sample	$\hat{\varepsilon}_S$	d_E [μm]	σ_E $[\Omega \cdot \text{cm}]^{-1}$	$\hat{\varepsilon}_E$
CMT 78 HgTe/CdHgTe	11.0 - 0.80 i	2.0	9.0	$-31 - 1.816 \cdot 10^3$ i
CMT 76 HgTe	11.0 - 0.45 i	1.2	38.5	$-197 - 7.770 \cdot 10^3$ i
Q 105 CdHgTe (0.17)	11.0 - 0.50 i	1.6	1470	$-8275 - 2.967 \cdot 10^5$ i
Q 107 CdHgTe (0.16)	11.0 - 11.0 i	2.9	1107	$-6226 - 2.234 \cdot 10^5$ i
Q 114 CdHgTe (0.175)	11.0 - 0.50 i	5.2	510	$-2858 - 1.029 \cdot 10^5$ i
Q 117 CdHgTe (0.21)	11.0 - 11.0 i	3.45	133	$-730 - 2.684 \cdot 10^4$ i
Q 118 CdHgTe (0.19)	11.0 - 0.50 i	2.4	236	$-1312 - 4.763 \cdot 10^4$ i
Q 132 CdHgTe/CdHgTe (0.70/0.20)	11.0 - 0.50 i	2.35	105	$-572 - 2.119 \cdot 10^4$ i
Q 153 CdHgTe (0.22)	11.0 - 11.0 i	2.5	55.9	$-295 - 1.128 \cdot 10^4$ i
Q 154 CdHgTe (0.22)	11.0 - 0.50 i	2.2	67.1	$-359 - 1.354 \cdot 10^4$ i

The theoretical considerations in the foregoing sections are the basis for the analysis of our experimental data. As discussed above, we measure the attenuation and the phase shift caused by the sample (cf. Fig. 1), and the theoretical results according to (11), i.e. the calculated values of the transmissioncoefficient, have to model these quantities. The microwave value of the conductivity is then determined from the intersection of the measured values of the attenuation A and the phase shift φ with their calculated dependence on the layer conductivity σ_E, $A = f(\sigma_E)$ and $\varphi = f(\sigma_E)$ (cf. Fig. 4). The input parameters for the calculation are compiled in Tables 1 and 2. Figure 8 shows, as an example, the graphic determination of σ_E for the samples Q 132 and Q 154. No corrections have been made. For Q 154, i.e. the sample with the lower conductivity, it is useful to determine σ_E from both A and φ. With respect to φ, the data in Fig. 8 show an offset, especially for sample Q 154, which is beyond the limits of experimental error of typically ±3% in this region. This phase offset is the difference between the independently determined van der Pauw value of σ_E (circles in Fig. 8) and the intersection of the microwave value (broken line in Fig. 8) with the curve $\varphi(\sigma_E)$ (full line in Fig. 8). For A, the agreement between van der Pauw value and microwave value is much better. In the case of sample Q 132, i.e. the sample with the higher conductivity, it is not recommended to use A for the determination of σ_E because $A(\sigma_E)$ has a maximum in the corresponding σ-range (cf. also Fig. 4). Therefore, we have to rely on φ in this case. but usually an accurate experimental determination of the phase shift is more difficult than that of the attenuation.

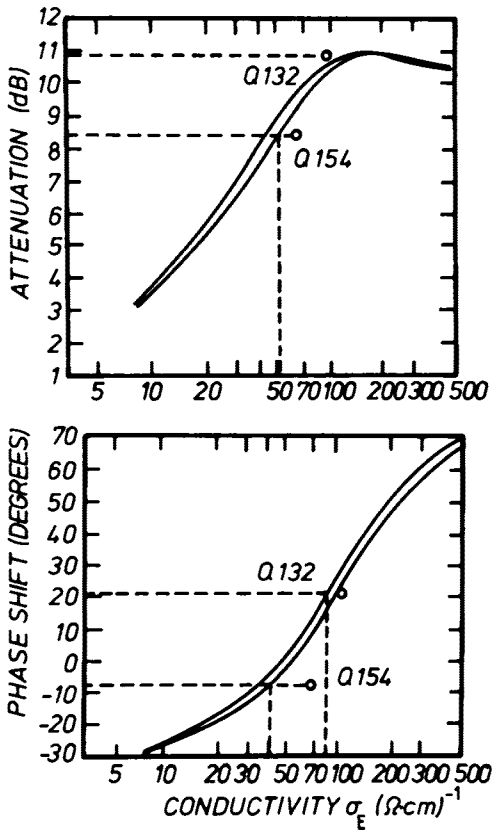

Fig. 8. Microwave determination of the layer conductivity σ_E for samples Q 132 and Q 154 (see Table 2 for their properties). Experimental data (broken lines) and calculated data (full lines) evaluated with $d_E = 2.2\,\mu m$ and $2.5\,\mu m$. For comparison, the van der Pauw conductivity is shown intersecting the experimental data (circles)

The relatively large phase offset observed in Fig. 8 can be explained by the fact that we have assumed an ideal electrical contact between the sample and the waveguide wall in our theoretical calculations. In the experiment, we have tried to improve the contact by inserting thin copper strips and/or electric conductivity paste between sample and wall of the waveguide. But an ideal contact cannot be achieved in this way. Other methods whichinvolve soldering etc. [9, 30] are not applicable for these thin layers which are produced in a nonequilibrium process. It is most probable that residual capacities lead to the phase differences [30]. On the other hand, the phase offsets are totally reproducible and seem to be typical for the corresponding conductivity range. This offers the possibility of empirical corrections. Another possibility to overcome this problem is to include a very thin air-gap in the calculations for a better modeling of the experimental data. We shall pursue this way in the future, even if this means a substantial extension of the theoretical considerations because not only TE_{m0} modes are to be considered but the whole set of TE_{mn} and TM_{mn} modes.

Before comparing these theoretical results with experimental data, some comments are necessary about the convergence of our calculation procedure. In this context, it is important to choose a sufficiently high number of modes N for the calculation, but not so high that the computing time would become unnecessarily long. The convergence has been tested at various steps of our procedure with the final results presented in Table 3, i.e. the transmission of the sample. This calculation has been performed for $\hat{\varepsilon}_S = 10.6 - 11.0\,i$, $\sigma_E = 500\,(\Omega cm)^{-1}$ ($\hat{\varepsilon}_E = -2805 - 1.010 \times 10^5\,i$) and $d_E = 2.0\,\mu m$. The results (Table 3) show that it is necessary to use 70 modes. For $\sigma_E < 100\,(\Omega cm)^{-1}$ however, the number of modes N can be reduced to 20. Due to the high attenuation of the modes in the sample region, the number of zig-zag-reflections k can be restricted to 4.

Table 3. Convergence properties of the theoretical calculations, depending on the number of modes N used for evaluating the transmission coefficient $|T/T_0|$, the attenuation A and the phase shift φ

N	$\lvert T/T_0 \rvert$	A [dB]	φ [degrees]
20	0.2490	10.61	66.43
30	0.2860	10.87	65.88
40	0.2841	10.92	65.53
50	0.2837	10.94	65.40
60	0.2834	10.952	65.30
70	0.2832	10.958	65.26

4 Comparison of Microwave-Determined and Transport-Determined Data

Under the conditions outlined above, we are able to calculate reliable theoretical data for comparison to the experimental results. In Table 4, such a comparison is made for various samples. In the two columns with the designation "experiment", we have listed the measured values of the phase shift φ and of the attenuation A. The two columns with the designation "theory" contain the corresponding data calculated using the parameter values in Tables 1 and 2, where σ_E is the van der Pauw value. With respect to A, the agreement is excellent for the whole conductivity range, although the values of φ agree well only for low layer conductivities. In the high conductivity range, however, there is the phase offset in excess of the experimental error, as discussed above. A large difference in the phase shift was observed for sample Q 118 (cf. Table 2). This phase offset is about 20° (not

Table 4. Experimental and theoretical results (attenuation A and phase shift φ) and the layer conductivity σ_E deduced from the microwave measurements (MW) compared with the van der Pauw conductivity (VdP)

Sample	Experiment		Theory		Conductivity σ_E	
	A [dB]	φ [degrees]	A [dB]	φ [degrees]	MW $[\Omega \cdot cm]^{-1}$	VdP $[\Omega \cdot cm]^{-1}$
CMT 78	3.25	-27	3.32	-27.6	8.7	9
CMT 76	5.3	-20	5.24	-20.0	40	38.5
Q 105	10.9	68	10.31	74.0	820	1470
Q 107	10.5	73	10.40	75.5	742	1107
Q 114	10.65	68	10.24	75.4	300	510
Q 117	11.3	42	11.41	52.4	93	133
Q 132	10.9	21	10.67	29.8	87	105
Q 153	10.8	10	11.14	17.3	48	56
Q 154	8.4	8	9.5	9.2	52	67

listed in Table 4) and, most probably, it is caused by structural defects such as inhomogeneous layer thicknes at the edges or across the sample which was determined by X-ray diffraction.

In the last two columns of Table 4, we present a comparison of the layer conductivity deduced from microwave measurements with the van der Pauw data. Generally, it has to be kept in mind, when comparing the data in Table 4, that the accuracy of this determination of the conductivity depends not only on the accuracy of the measurement of A and φ but is also influenced by the experimental errors in the measurement of $\hat{\varepsilon}_S$ of the substrate and of d_E of the layer (up to 20%), as well as by the errors in the van der Pauw measurement. Apart from the phase-offset, the data in Fig. 8 and in Table 4 show that the contactless microwave method yields values for the conductivity of the layer which are within the limits of tolerable experimental error.

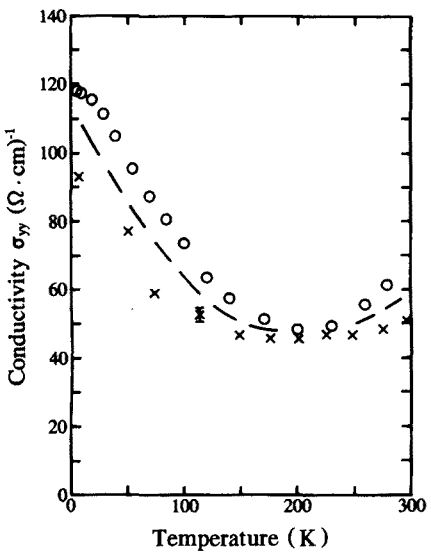

Fig. 9. Layer conductivity σ_{yy} (real part) of sample Q 154 as a function of temperature: Microwave-determined (×) and van der Pauw data (○)

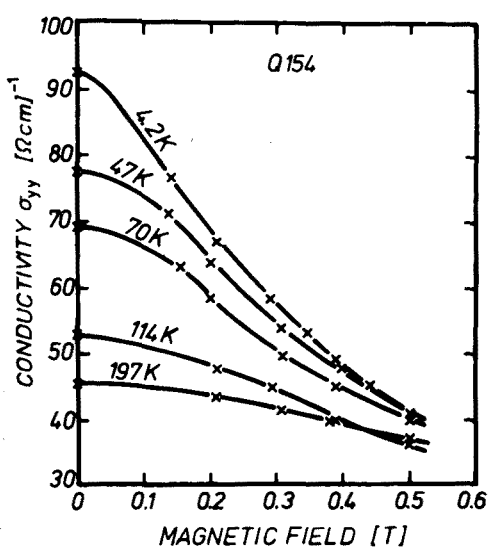

Fig. 10. Layer conductivity σ_{yy} (real part) of sample Q 154 vs magnetic field for several temperatures. The solid lines are guide to the eye

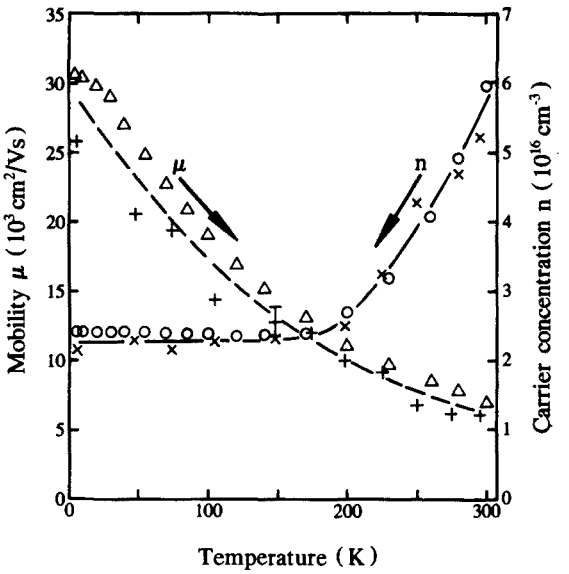

Fig. 11. Mobility μ and carrier concentration n for sample Q 154 vs temperature; evaluated from the microwave data of Figs. 9 and 10: n (×) and μ (+); and for comparison from transport data: n (○) and μ (△). In both cases, a one carrier model has been used

For one sample (Q 154), as an example, the conductivity has been mesured with the contactless microwave method as a function of temperature and magnetic field. The results of these galvanomagnetic measurements are compared to van der Pauw transport data, also available for this sample. The conductivities at various temperatures were derived in the way outlined above (cf. Fig. 8) by taking into account the measured temperature dependence of $\check{\varepsilon}_S$ of the substrate. It is worthwhile mentioning that the conductivity of the substrates did not show any measurable dependence on the magnetic field. This is due to the low mobility of the carriers. On the other hand, the conductivity of the substrate decreases very strongly with decreasing temperature due to a decrease of the carrier concentration.

Figure 9 shows the layer conductivity of sample Q 154 as a function of temperature. In an applied magnetic field, the conductivity $\hat{\sigma}_{yy}$ always decreases with increasing magnetic field because of the denominator in (13). This is shown in Fig. 10 for several temperatures. The dependence of $\hat{\sigma}_{yy}$ on the magnetic field B can be used to evaluate the mobility μ of the carriers in the layer using (13). Then the carrier concentration n is determined by means of (15). The results are shown in Fig. 11. The corresponding data obtained with the conventional method (van der Pauw, employing a one carrier model) are also presented in Fig. 9 and Fig. 11. Comparison shows that the microwave values for σ_{yy}, μ, and n agree quite well with the van der Pauw data. Only for high conductivities and mobilities at low temperatures, the agreement could probably be improved by solving the above mentioned air-gap problem. Generally, the mobility of the sample Q 154 is lower by a factor of three as compared to data reported for high quality bulk material and epitaxial layers [31–33].

5 Conclusions

The conductivity of CdHgTe epitaxial layers has been measured by means of the microwave technique of the partially filled waveguide. The essential characteristics of the wave propagation in this configuration have been determined by a multi-mode matching procedure. We have discussed in detail the behaviour of the transmission coefficient and the field configuration in dependence on the layer conductivity, the layer thickness and the electrical properties of the substrate. All our results show that the procedure of multi-mode matching has to be used for every sample, even for substrates and epitaxial layers with low conductivities. Otherwise, we do not obtain correct and reliable results. The assumption of a hardly disturbed TE_{10} mode has proven to be inadequate. The theoretical results are verified excellently by experiment and they are in total agreement with recent theoretical calculations based on a multi-mode network analysis [23].

Using the contactless microwave method with the calculated results as a basis for the analysis of the experimental data, the conductivities of epitaxial layers of II–VI compounds have been determined with an accuracy comparable to van der Pauw transport measurement. With the help of an external magnetic field not only conductivities but also mobilities and carrier concentrations have been determined over a large temperature range. These studies of the electrical properties as a function of magnetic field and temperature offer the possibility for detailed investigations of the transport properties with respect to the presence of more than one type of carrier.

There are still problems which have to be and will be solved in the near future. First, a theoretical treatment including an air-gap between the sample and the waveguide is necessary to circumvent the contact problems and to improve accuracy. Second, the influence of the E_z component originating from an applied magnetic field should be studied in more detail, especially with respect to the changes in the field distribution and thus in the measured conductivity. There are experimental indications that this influence is not negligible for very high layer mobilities. In addition, this extension of the method will offer the possibility of investigating the off-diagonal component $\hat{\sigma}_{xy}$ of the conductivity tensor.

Acknowledgements. Financial support of the Bundesministerium für Forschung und Technologie (BMFT) in connection with the project "layer structures and devices from II–VI semiconductors" and helpful discussions with Prof. Dr. G. Landwehr are gratefully acknowledged.

References

1. R.N. Bicknell, N.C. Giles, J.F. Schetzina: Appl. Phys. Lett. **49**, 1095 (1986)
2. R.N. Bicknell, N.C. Giles, J.F. Schetzina: Appl. Phys. Lett. **49**, 1735 (1986)
3. K. Zanio: Cadmium Telluride. In *Semiconductors and Semimetals*, Vol. 13 (Academic, New York 1978)
4. W. Bauhofer: J. Phys. E: Sci. Instrum. **14**, 934 (1981)
5. N.P. Ong: J. Appl. Phys. **48**, 2935 (1977)
6. N.P. Ong, P. Monceau: Phys. Rev. B **16**, 3443 (1977)
7. N.P. Ong, W. Bauhofer, C.J. Wei: Rev. Sci. Instrum. **52**, 1367 (1981)
8. H.M. Altschuler: Dielectric Constant. In *Handbook of Microwave Measurements*, ed. by M. Sucher, J. Fox (Wiley, New York 1963)
9. K.H. Seeger: J. Appl. Phys. **63**, 5439 (1988)
10. W. Jantz, T. Frey, K.H. Bachmann: Appl. Phys. A **45**, 225 (1988)
11. R. Meisels, f. Kuchar: Z. Phys. B: Cond. Mat. **67**, 443 (1987)
12. F. Kuchar: Festkörperprobleme **28**, 45 (1988)
13. F. Koch: Surf. Sci. **58**, 104 (1976)
14. F. Koch: Surf. Sci. **80**, 110 (1979)
15. H. Lehmann, G. Nimtz, L.D. Haas, T. Jakobus: Appl. Phys. **25**, 291 (1981)
16. G. Nimtz, R. Dornhaus, M. Schifferdecker, I. Shih, E. Tyssen: J Phys. E: Sci. Instrum. **11**, 1109 (1978)
17. J. Schwinger, D.S. Saxon: Discontinuities in Waveguides. In *Documents of Modern Physics* (Gordon and Breach, New York 1968)
18. S. Sridhar, D. Reagor, G. Gruner: Rev. Sci. Instrum. **56**, 1946 (1985)
19. Tae Wan Kim, W.P. Beyermann, D. Reagor, G. Gruner: Rev. Sci Instrum. **59**, 1219 (1988)
20. W.V. McLevige, T. Itoh, R. Mittra: IEEE Trans. MTT-**23**, 788 (1975)
21. Feng Zheng-he: Science in China (Series A) **32**, 983 (1989)
22. Xu Shanjia: J. Electron. **6**, 232 (1989)
23. Xu Shanjia, Wu Xinzhang, P. Greiner, C.R. Becker, R. Geick: Int' J. of Infrared and Millimeter Waves **13**, 569 (1992)
24. R.S. Brazis, J.K. Furdyna, J.K. Pozela: Phys. Stat. Sol. (a) **53**, 1 (1979); Phys. Stat. Sol. (a) **54**, 11 (1979)
25. E.D. Palik, J.K. Furdyna: Rep. Progr. Phys. **33**, 1193 (1970)
26. I. Strzalkowski, S. Joshi, C.R. Crowell: Appl. Phys. Lett. **28**, 350 (1976)
27. A. Waag, Y.S. Wu, R.N. Bicknell-Tassius, C. Gonser-Buntrock, G Landwehr: J. Appl. Phys. **68**, 212 (1990)
28. L.J. van der Pauw: Philips Res. Rep. **13**, 1 (1958)
29. J. Brice, P. Capper (eds.): Properties of Mercury Cadmium Tel luride, EMIDS Dataviews Series No. 3 (INSPEC, London 1987 p. 29
30. K.S. Champlin, G.H. Glover: J. Appl. Phys. **37**, 2355 (1966)
31. K.A. Harris, S. Hwang, Y. Lansari, J.W. Cook, Jr., J.F. Schetzina M. Chu: J. Vac. Sci. Technol. A **5**, 3085 (1987)
32. W. Scott: J. Appl. Phys. **43**, 1055 (1972)
33. R.N. Bicknell-Tassius, S. Scholl, C. Becker, G. Landwehr: In *High Magnetic Fields in Semiconductor Physics III*, Springer Ser. Solid State Sci., Vol. 101 (Springer, Berlin, Heidelberg 1992) p. 386